Journal of proteome research

pubs.acs.org/jpr

Article

Next-Generation Serology by Mass Spectrometry: Readout of the SARS-CoV-2 Antibody Repertoire

Rafael D. Melani, Benjamin J. Des Soye, Jared O. Kafader, Eleonora Forte, Michael Hollas, Voislav Blagojevic, Fernanda Negrão, John P. McGee, Bryon Drown, Cameron Lloyd-Jones, Henrique S. Seckler, Jeannie M. Camarillo, Philip D. Compton, Richard D. LeDuc, Bryan Early, Ryan T. Fellers, Byoung-Kyu Cho, Basil Baby Mattamana, Young Ah Goo, Paul M. Thomas, Michelle K. Ash, Pavan P. Bhimalli, Lena Al-Harthi, Beverly E. Sha, Jeffrey R. Schneider, and Neil L. Kelleher*

Cite This: https://doi.org/10.1021/acs.jproteome.1c00882

Read Online

ACCESS | Metrics & More | Article Recommendations | Supporting Information

ABSTRACT: Methods of antibody detection are used to assess exposure or immunity to a pathogen. Here, we present Ig-MS, a novel serological readout that captures the immunoglobulin (Ig) repertoire at molecular resolution, including entire variable regions in Ig light and heavy chains. Ig-MS uses recent advances in protein mass spectrometry (MS) for multiparametric readout of antibodies, with new metrics like Ion Titer (IT) and Degree of Clonality (DoC) capturing the heterogeneity and relative abundance of individual clones without sequencing of B cells. We applied Ig-MS to plasma from subjects with severe and mild COVID-19 and immunized subjects after two vaccine doses, using the receptor-binding domain (RBD) of the spike protein of SARS-CoV-2 as the bait for antibody capture. Importantly, we report a new data type for human serology, that could use other antigens of interest to gauge immune responses to vaccination, pathogens, or autoimmune disorders.

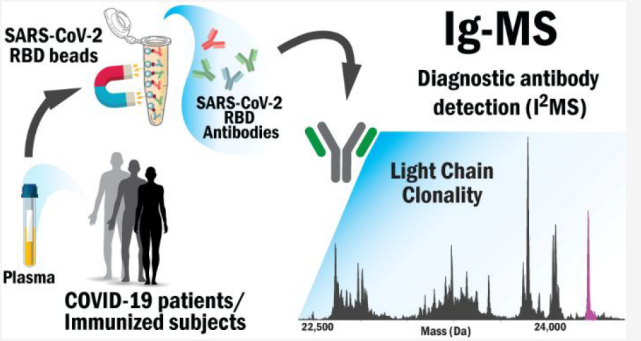

KEYWORDS: *antibodies, SARS-CoV-2, COVID-19, top-down mass spectrometry, serology, proteomics, individual ion mass spectrometry*

INTRODUCTION

Since late 2019, severe acute respiratory syndrome coronavirus 2 (SARS-CoV-2) and its associated disease COVID-19[1] have been at the center of a global pandemic affecting more than 200 million people, especially immunocompromised individuals, the elderly, and individuals with pre-existing conditions.[2] This has resulted in more than 5 million deaths worldwide, including >700,000 in the USA where COVID-19 has become a leading cause of death.[3,4] Unfortunately, the global death toll is still high due to delays in vaccination and the emergence of more transmissible variants of SARS-CoV-2, against which the available vaccines and antibody-based therapeutics may be less effective.[4]

Most COVID-19 patients develop antibodies against SARS-CoV-2 within a few weeks after infection,[5,6] commonly recognizing targets such as viral envelope, nucleocapsid, and spike proteins. In particular, the spike protein receptor-binding domain (RBD) is a robust immunogenic target that has been the focus of many antibody-based diagnostics and therapeutics against SARS-CoV-2.[7]

Generally, standard serology tests (e.g., ELISA and lateral flow assays) can reliably detect whether a patient possesses antibodies against a target antigen, but they do not capture the clonality and makeup of an entire immunoglobulin (Ig) repertoire. A more precise assessment of immune status relative to SARS-CoV-2 at single clone resolution would significantly improve serological testing capabilities. A proteomics approach to the antibody repertoire has been challenging, though digestion-based approaches combined with Ig-seq have been evaluated and attempted.[8,9] Several studies have used a low-resolution view of the IgG landscape using peptide-based analyses of IgGs after tryptic digestion,[10,11] including one conducted in the COVID-19 context.[12,13]

Intact proteins have many proteoforms,[14] and in the case of antibody heterogeneity, this could be captured if there was a molecular readout with enough resolution and specificity. Past

Received: November 14, 2021

efforts have been able to detect monogammapathies (e.g., B cell cancers like multiple myeloma[15]), but a direct readout of Ig repertoire at high resolution is not currently possible. Addressing this, here we establish Ig-MS, which isolates antibodies against a specific target from the plasma of patients and controllably breaks them down into their heavy and light chains (HC and LC). Once created, HC and LC are analyzed by individual ion mass spectrometry (I^2MS). This approach generates tractable spectral outputs for extremely heterogeneous intact or fragmented protein samples (under denatured or native conditions) directly in the mass domain that are uninterpretable under traditional ensemble analysis due to extensive charge state overlap in the m/z domain.[16−18] Accurate charge detection of individual ions using STORI plot analysis are completed routinely on ∼500 fold more dilute samples than classical protein MS analysis with the collection of hundreds of individual ions per acquisition event.[16,19] An additional advantage of individual ion analysis includes ∼20× resolution gains over ensemble ion analysis which further advances the deconvolution of complex mixtures.[20,21]

Here, we apply Ig-MS to generate compositional profiles for Ig repertoires, their degree of clonality, and titers for an initial cohort of COVID-19 subjects. With increased resolution for molecular serology, Ig-MS could provide high-value clinical correlates of viral neutralization, the presence, extent, and course of the disease, and/or assess the degree of protection after COVID-19 vaccination.

EXPERIMENTAL SECTION

Patient Cohorts and Plasma Sampling

Throughout this work, plasma from convalescent COVID-19 donors and those in control groups were collected under IRB NUMBER 00000482 by the clinical team at Rush University Medical Center. Patients were sampled post-infection 10 or more days after symptom onset. Three uninfected subjects that never had contact with COVID-19 were used as negative controls. These individuals were vaccinated using the BNT162b2 vaccine from Pfizer Inc. and BioNTech, and plasma samples were collected 20 days after the first shot and 28 days after the second shot (booster). Plasma was isolated from the blood collected using tubes with sodium heparin (BD 367874, Fisher Scientific) by centrifugation at 1,500 × g for 10 min. Plasma from a convalescent patient featuring a high titer of anti-SARS-CoV-2-RBD antibodies was purchased from AllCells (commercial sample 1 − CS1) and used as a standard positive control throughout the study. As a negative control/blank background, pooled serum collected before the emergence of the SARS-CoV-2 pandemic was used (Fisher Scientific BP2657100 UNSPSC 12352207, purchased 05/05/2019).

RBD-Binding by ELISA

Hisorb Ni^+ plates (Qiagen) were coated with 100 μL of His-tagged RBD (BEI) at a concentration of 2 μg/mL overnight at 4 °C. Plates were blocked with 100 μL per well of 3% nonfat milk prepared in PBS with 0.1% Tween 20 (PBST) added to the plates at room temperature for 1 h. Next, heat-inactivated plasma from COVID-19 patients was diluted 1:10 in PBS and added at 100 μL per well for 2 h at RT. Plates were washed with PBS-T 3 times, followed by incubation with secondary anti-human IgG Fc HRP (1:4,000) for 1 h. Plates were washed 3 times with PBS-T followed by the addition of TMB substrate for 10 min. The reaction was stopped using 3 M HCl and read at OD 450 nm on the Biotek Cytation 3.

SARS-CoV-2 Surrogate Virus Neutralization Assay

COVID-19 patient plasma samples were heat-inactivated at 56 °C for 1 h. Following heat inactivation, samples were diluted at a volume ratio of 1:9 in sample dilution buffer and mixed with a 1:1,000 HRP-conjugated RBD solution in HRP dilution buffer at a volume ratio of 1:1 and incubated at 37 °C for 30 min. Following incubation, samples and kit-provided controls were added to an ACE2-coated 96-well plate, 100 μL/well in duplicate, and incubated at 37 °C for 15 min. The plate was then washed four times with 1× wash solution and incubated with 100 μL/well TMB solution in the dark at room temperature for 15 min, followed by the addition of 50 μL/well reaction stop solution. The absorbance was then read on a biotek Cytation 3 plate reader at 450 nm. The protocol is adapted from GenScript SARS-CoV-2 Surrogate Virus Neutralization Test Kit (Cat. No. L00847-A), and all reagents used were provided in the test kit.

Recombinant Monoclonal Antibody

Human recombinant monoclonal Anti-SARS-CoV-2 antibody, mAb CR3022 produced in *Nicotiana bethamiana* (tobacco plant) was obtained from Novici Biotech LLC (Lot NCV_051520B) as a 1.0 mg/mL solution in PBS (pH 7.2). This reagent binds RBD of the Spike protein from SARS-CoV-2 and is also available through BEI Resources, catalog number NR-53876. The recombinant mAb was stored at 4 °C prior to use.

Recombinant Expression of SARS-CoV-2 Spike Protein Receptor-Binding (RBD) Domain

The plasmid pCAGGS SARS-CoV-2 RBD comprises an N-terminal signal sequence, amino acids 319−541 of the spike protein from SARS-CoV-2 (the receptor-binding domain, RBD), and a C-terminal 6-His tag.[22] This vector was obtained from BEI Resources (BEI NR-52309) and expressed recombinantly using the Expi293 Expression System as follows: Expi293F cell culture (1 L total) was maintained in a 37 °C incubator with ≥80% relative humidity, 8% CO_2 on an orbital shaker platform, and subcultured at cell density (3−5) × 10^6 viable cells/mL. One day before transfection, the cells were seeded to a final density of 2.5 × 10^6 viable cells/mL and allowed to grow overnight. On the day of transfection, the culture was diluted to 3 × 10^6 viable cells/mL with fresh, prewarmed Expi293 Expression Medium. The transfection was performed using ExpiFectamine 293 Transfection Kit. Briefly, DNA/Opti-MEM I and ExpiFectamine 293/Opti-MEM I mixtures were prepared separately and incubated at room temperature for 5 min. These mixtures were then combined, and the total complexation mixture was incubated at room temperature for another 20 min after which it was slowly mixed into the cell culture to initiate transfection. Eighteen hours post-transfection, ExpiFectamine 293 Transfection Enhancer 1 and ExpiFectamine 293 Transfection Enhancer 2 were added to the culture. The cell culture supernatant was collected after 6 days and prepared for purification.

Purification of SARS-CoV-2 RBD

Purification was performed on AKTAxpress (GE Healthcare Life Science) FPLC purification system. Clarified cell culture supernatant was loaded onto HisTrap FF 5 mL column (GE Healthcare Life Science, Cat #17-5255-01). The column was washed twice, once with binding buffer (10 mM Tris-HCl, 500

https://doi.org/10.1021/acs.jproteome.1c00882
J. Proteome Res. XXXX, XXX, XXX−XXX

mM NaCl, pH 7.4) and then with binding buffer +12.5 mM imidazole to remove unspecifically bound material. Finally, bound RBD protein was eluted off the column with elution buffer (10 mM Tris-HCl, 500 mM NaCl, 500 mM imidazole, pH 7.4). Column loading, washes, and elution were all performed at a 3 mL/min flow rate. After elution, the collected fraction was buffer exchanged into 1× PBS.

RBD Validation by Bottom-Up Proteomics

Fifty migrograms of RBD was acetone/TCA precipitated with 8 volumes of cold acetone and 1 volume of trichloroacetic acid overnight at −20 °C. After washing the pellet with ice-cold acetone, the resulting protein pellet was resuspended into 50 μL of 8 M urea in 400 mM ammonium bicarbonate, pH 7.8, reduced with 4 mM dithiothreitol at 50 °C for 30 min, and cysteines were alkylated with 18 mM iodoacetamide in the dark for 30 min. The solution was then diluted to <2 M urea (final concentration), and trypsin (Promega) was added at a final trypsin/protein ratio of 1:50 prior to overnight incubation at 37 °C with shaking. The resulting peptides were desalted using solid-phase extraction on a Pierce C18 Spin column and eluted in 80 μL of 80% acetonitrile (ACN) in 0.1% formic acid (FA). After lyophilization, peptides were reconstituted with 5% ACN in 0.1% FA.

Peptides were analyzed by LC-MS/MS using a Dionex UltiMate 3000 Rapid Separation nanoLC and a Q Exactive HF Hybrid Quadrupole-Orbitrap Mass Spectrometer (Thermo Fisher Scientific Inc., San Jose, CA). Approximately 1 μg of peptide sample was loaded onto the trap column, which was 150 μm × 3 cm in-house packed with 3 μm ReproSil-Pur C18 beads (Maisch, GmbH, Germany). The analytical column was a 75 μm × 10.5 cm PicoChip column packed with 3 μm ReproSil-Pur C18 beads (New Objective, Inc. Woburn, MA). The flow rate was kept at 300 nL/min. Solvent A was 0.1% FA in water, and Solvent B was 0.1% FA in ACN. The peptides were separated on a 120 min analytical gradient from 5% ACN/0.1% FA to 40% ACN/0.1% FA. The mass spectrometer was operated in a data-dependent mode. The source voltage was 2.40 kV, and the capillary temperature was 320 °C. MS^1 scans were acquired from 300 to 2,000 m/z at 60,000 resolving power and automatic gain control (AGC) set to 3×10^6 charges. The top 20 most abundant precursor ions in each MS^1 scan were selected for fragmentation. Precursors were selected with an isolation width of 2 m/z and fragmented by Higher-energy collisional dissociation (HCD) at 30% normalized collision energy in the HCD cell. Previously selected ions were dynamically excluded from reselection for 20 s. The MS^2 minimum AGC was set to 1×10^3.

Proteins were identified from the tandem mass spectra extracted by Xcalibur version 4.0. MS^2 spectra were searched against the Spike protein RBD and SwissProt *Homo sapiens* database using Mascot search engine (Matrix Science, London, UK; version 2.7.0). All searches included carbamidomethyl cysteine as a fixed modification, oxidized methionine, deamidated asparagine/glutamine, and acetylated *N*-terminal as variable modifications. Three missed tryptic cleavages were allowed. The MS^1 precursor mass tolerance was set to 10 ppm, and the MS^2 tolerance was set to 0.05 Da. The search result was visualized by Scaffold v 5.0 (Proteome Software, INC., Portland, OR). A 1% false discovery rate cutoff was applied at the peptide level. Only proteins with a minimum of two unique peptides above the cutoff were considered identifications.

Fabrication of RBD-Loaded Magnetic Beads

Recombinantly expressed RBD was covalently loaded onto Dynabeads MyOne Carboxylic Acid beads (Thermo 65011, Thermo 65012) according to the manufacturer-provided protocol for "Two-Step Coating Procedure using NHS". In brief, for a single preparation, 1.5 mL of bead suspension was dispensed and washed twice with 1.5 mL of 25 mM MES, pH 6.0 for 10 min at room temperature. Following washes, bead chemistry was activated by suspending the beads into 1.5 mL of freshly prepared 50 mg/mL *N*-hydroxysuccinimide (NHS), mixing in 1.5 mL of freshly prepared 50 mg/mL 1-ethyl-3-(3dimethylaminopropyl) carbodiimide (EDC), and incubating for 30 min at room temperature. Following activation, the beads were again washed twice with 1.5 mL of 25 mM MES, pH 6.0 for 10 min at room temperature. Activated beads were suspended into 1 mL 25 mM MES, pH 6.0 to which 1.5 mg of RBD protein was added. The sample was mixed and incubated for 30 min at room temperature. Next, the beads were pulled down, the supernatant was discarded, and loading was quenched by incubating the beads in 1 mL of 50 mM Tris, pH 6.8, for 15 min at room temperature. After quenching, beads were washed four times in 1 mL 1× PBS + 0.1% human serum albumin (HSA), and finally suspended into 3 mL 1× PBS + 0.1% HSA for storage at 4 °C.

Enrichment of RBD-Reactive Antibodies from Patient Samples

Antibody pull-downs were assembled by combining 100 μL of patient plasma/serum with 35 μL of RBD-loaded bead suspension and diluting to a volume of 1 mL with 1× TBS. Assembled pull-downs were incubated overnight at 4 °C with end-overend mixing. After this, incubation beads were pulled down, supernatant was removed, and beads were resuspended into 1 mL wash buffer (1× TBS + 0.1% Tween + 1% NP-40 + 1% NP-40 substitute). Suspensions were transferred onto a KingFisher Flex for additional 4 washes in 1 mL wash buffer, 2 washes in 1 mL 1× TBS, and a 30 min incubation in 100 μL 100 mM glycine, pH 11.5 + 0.1% sodium deoxycholate at 37 °C to elute antibodies associated with bead-bound RBD. For LC/Fd workflow, Ig-pull-downs included an on-bead IdeS digestion of RBD-binding antibodies. This involved an additional incubation step between the first and second 1× TBS washes, during which beads were incubated in 100 μL of 50 mM sodium phosphate +150 mM sodium chloride (pH 6.6) in the presence of 200 U IdeS enzyme (Promega V751A) for 3.5 h at 37 °C.

Preparation of Enriched Antibodies for Individual Ion Mass Spectrometry

Following elution, 100 ng of mAb CR3022 standard antibody was added to each elution fraction to serve as an internal standard across all samples. For samples including an IdeS digest step, the mAb CR3022 standard underwent an in-solution IdeS digestion according to manufacturer protocols prior to being added to pull-down elution fractions. After supplementation with standard antibody, each fraction was combined with 160 μL 8 M urea and 25 μL 1 M TCEP, mixed, and set to incubate for 1 h at room temperature to facilitate the complete denaturation of the Ig-RBD and permit the complete reduction of all inter- and intrachain disulfide bonds. Following incubation, reduced antibody fragments were cleaned via methanol−chloroform−water precipitation as has been previously described.[23,24]

https://doi.org/10.1021/acs.jproteome.1c00882
J. Proteome Res. XXXX, XXX, XXX−XXX

Visualization of RBD-Binding Antibodies via Western Blot

Fractions of interest were combined with Bolt loading buffer (final concentration 1×, Thermo Fisher B0007) and dithiothreitol (DTT, final concentration 100 mM) and incubated at 100 °C for 10 min. Boiled samples were loaded onto a 4−12% Bolt Bis-Tris Plus polyacrylamide gel, which was run in a Mini Gel Tank (Thermo Fisher A25977) using MES running buffer for 1 h at 120 V. Next, the gel was trimmed, and proteins were transferred to a nitrocellulose membrane using iBlot 2 nitrocellulose transfer stacks (Thermo Fisher IB23001) on an iBlot 2 Dry Blotting System following manufacturer instructions. The transfer method used was the templated method P3 (20 V for 7 min). After transfer, the membrane was blocked using 1× TBS + 0.05% Tween + 5% milk for 1 h at room temperature with mixing. After 1 h, goat anti-human IgG (H+L) HRP conjugate (Thermo Fisher 31410) was added directly to the milk at a 1:20,000 dilution, and the membrane was moved to 4 °C to incubate overnight. The next day, the milk + antibody mixture was discarded, and the membrane was washed 3× in 1× TBS + 0.05% Tween for 5 min at room temperature with mixing. Finally, the blot was imaged on an iBright CL1000 imager (Thermo Fisher) using 800 μL of Immobilon Classico Western HRP substrate (Millipore Sigma WBLUC0500).

Western Blot Identification of Enriched Antibody Isotypes

An enrichment was performed as described in the section Enrichment of RBD-Reactive Antibodies from Patient Samples to screen for the presence of individual human antibody isotypes (IgG1, IgG2, IgG3, IgG4, IgA, IgD, IgE, and IgM). In this case, after elution, the fraction was divided into 8 equal parts. Positive controls were assembled for each isotype being examined, with each control consisting of 250 ng of a commercially obtained purified antibody of that isotype (IgG1: Sigma AG502; IgG2: Sigma I5404; IgG4: Sigma I4640; IgA: Sigma I4036; IgD: Sigma 401164; IgE: Sigma 401152; IgM: Sigma I8260). Negative controls for each isotype were assembled by combining 300 ng of all commercially obtained purified antibody isotypes omitting the specific isotype that the control was. Eluted material, positive, and negative controls were run in polyacrylamide gels, and proteins were transferred to nitrocellulose and blocked as described above. After blocking, each membrane was introduced to a primary antibody that specifically recognized the isotype of the antibodies being examined on that membrane (IgG1: AbCam ab108969; IgG2: AbCam ab134050; IgG3: AbCam ab109761; IgG4: AbCam ab109493; IgA: AbCam ab124716; IgD: AbCam ab124795; IgE: AbCam ab195580; IgM: AbCam ab134159) mixed with 1× TBS + 0.05% Tween + 5% milk. Primary antibodies were present at a dilution of 1:10,000. Membranes were incubated in primary antibodies overnight at 4 °C with mixing. The next day, primary antibody + milk was discarded, and all membranes were washed 3× in 1× TBS + 0.05% Tween for 5 min at room temperature with mixing. After washing, all membranes were submerged into 1x TBS + 0.05% Tween + 5% milk to which secondary antibody (Gt-anti-Rb-HRP (Sigma AP307P) had been added at a dilution of 1:5,000. Membranes incubated in secondary antibody for 1 h at room temperature with mixing, after which they were washed 3× in 1× TBS + 0.05% Tween for 5 min at room temperature with mixing and imaged as described above.

Anti-RBD Antibody Quantification

Titers of antibodies from patient plasma responsive to SARS-CoV-2 RBD were measured using Lumit Dx SARS-CoV-2 Immunoassay (Promega VB1080). Plasma from each patient was diluted 1:10 in 1× TBS and incubated at 56 °C for 1 h to inactivate any potential pathogens remaining. Following heat inactivation, samples were used as input and analyzed in triplicate using the assay following manufacturer protocols.

Individual Ion Mass Spectrometry

After precipitation, reduced antibody samples were redissolved in 200 μL of a 40% ACN and 0.5% acetic acid. A total of 70 μL of the sample was sprayed through an Ion Max Source (Thermo Fisher Scientific) fitted with a HESI II probe at a flow rate of 1 μL/min delivered by a PAL3 robot (CTC Analytics) and analyzed by a Q Exactive Plus mass spectrometer (Thermo Fisher Scientific).[25,26] Instrumental conditions included eFT off, pressured setting of 0.5, 1 kV orbitrap central electrode voltage, a spray voltage of 3.0 to 4 kV, sheath gas of 2 L/min, an in-source collision-induced-dissociation value of ∼15 V, and a source temperature of 320 °C. Injection times ranged from 1 to 400 ms and were optimized on a per-sample basis to collect hundreds to thousands of individual ions (depending on spectral complexity) per acquisition event to perform I^2MS analysis. Data were acquired from 650 to 2,500 m/z range for 70 min using 140,000 of resolving power (at 200 m/z).

Previously, I^2MS analysis has been demonstrated using an Orbitrap mass analyzer.[16,27,28] Briefly, I^2MS is a novel approach capable of discerning the mass profile of highly complex mixtures not amenable to venerable approaches used in protein mass spectrometry. Rather than measuring in the mass-to-charge (m/z) domain, I^2MS accurately determines the charge on each individual ion collected through a process called STORI plot analysis. STORI plot analysis, the determination of the slope of individual ion signal accumulation, was completed on each ion as a function of its specific frequency.[16] To simplify this process and reduce file sizes, only time-domain signals at specific frequencies where individual ions occurred, called STORI files, were recorded on an acquisition-to-acquisition basis. Each acquired STORI file was then processed to accurately determine the m/z and charge for every individual ion signal detected.

In order to evaluate the lower limits of the Ig-MS platform, we analyzed NIST antibody standard in a serial dilution series. All samples were infused at 1 μL/min for 50 min such that the same number of transients would be acquired for each experiment. Additionally, the injection time was scaled inversely to the sample concentration in order to maintain a constant per-cycle injection of 12.5 pg. For example, the 500 nM run used an injection time of 10 ms, and the 100 nM run used an injection time of 50 ms.

Proteoform Quantification for Light Chain, Fd, and Heavy Chain

I^2MS STORI files were processed to create mass spectra as .mzml files. Briefly, STORI files containing single ion peak information and transient sections are processed using a short-time Fourier transform (STFT) to assign slopes to single ions.[29] After slope assignment, charges were assigned to individual ion using an iterative voting algorithm, and spectra were generated using a normal kernel density estimate (KDE) and exported as either profile or centroided *.mzml* files.

https://doi.org/10.1021/acs.jproteome.1c00882
J. Proteome Res. XXXX, XXX, XXX−XXX

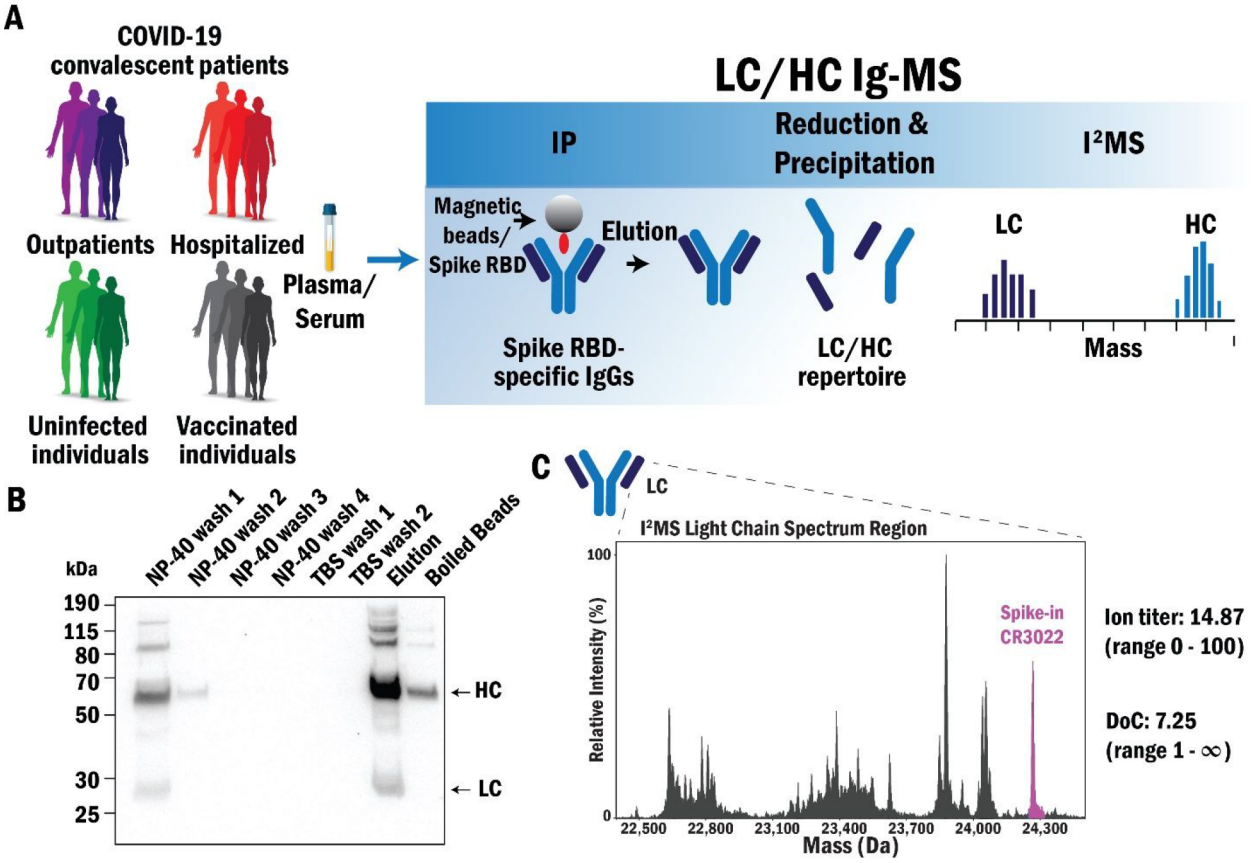

Figure 1. Ig-MS, a new platform for COVID-19 serology. (A) Overview of sample preparation and readout. Antibodies against the RBD domain of the SARS-CoV-2 spike protein are enriched from plasma or serum of COVID-19 patients, vaccinated, and control individuals using magnetic beads conjugated with RBD. The eluates are then reduced to obtain light (LC) and heavy chains (HC), which are analyzed by individual ion mass spectrometry (I^2MS). (B) Western blot showing the enrichment of Ig targeting SARS-CoV-2 spike RBD from CS1. (C) Example data set and metrics obtained from Ig-MS of the plasma from a COVID-19 convalescent patient (COVID-19_3) (only LC is shown).

Calculation of Ig-MS Ion Titer, Degree of Clonality, and Spectral Correlation Coefficients

Ig-MS ion titers were calculated using a custom script, in which *.mzml* I^2MS files were centroided and spectra divided into regions; the LC region, the regions of the standard peaks, and either the Fd fragment or HC regions for samples that were reduced with and without IdeS digestion, respectively. An average noise was calculated over these regions, and the sum was subtracted from the intensity for the region's total.[30] The titers were obtained by determining the ratio between the sum of the standard peak regions and the regions for the LC and Fd/HC regions, divided by the value of the spike-in standard, as shown in eq 1.

Ig-MS Ion Titer (IT)

$$\mathrm{IT} = \left\{\left[\sum_{\mathrm{LC\,min}}^{\mathrm{LC\,max}} (\mathrm{intensity} - \mathrm{noise}) + \sum_{\mathrm{Fd/HC\,min}}^{\mathrm{Fd/HC\,max}} (\mathrm{intensity} - \mathrm{noise})\right] \Big/ \left[\sum_{n}\left[\sum_{\mathrm{std\,peak\,n\,min}}^{\mathrm{std\,peak\,n\,max}} (\mathrm{intensity} - \mathrm{noise})\right]\right]\right\} / \mathrm{Std.\,mass}(\mu g) \quad (1)$$

The degree of clonality (DoC) was calculated by centroiding profile spectra for a given mass window corresponding to the LC region. First, the highest centroid peak is determined and using an averagine distribution, a window is created around the peak.[31] To account for simple adducts (+Na and $-H_2O$) the window was extended +39 and −18 Da. The intensities in this range are summed and divided by the total sum of all intensities in the LC region and inverted yield the DoC, as in eq 2. This metric takes a value of one to infinity, with the higher the number, the more complex the spectrum.

Degree of Clonality

$$\mathrm{DoC} = \frac{\sum_{\mathrm{LC\,min}}^{\mathrm{LC\,max}} \mathrm{intensity}}{\sum_{\mathrm{peak\,window\,min}}^{\mathrm{peak\,window\,max}} \mathrm{intensity}} \quad (2)$$

Spectral correlation coefficients were calculated for two spectra by taking centroided spectra and creating a padded array of equal length for each. Each peak in each centroided spectrum was fitted to a Normal KDE and summed into the padded arrays, yielding two Gaussian fitted spectra of equal length with indexes corresponding to the same mass. Calculating the cosine similarity using eq 3 yielded the spectral correlation coefficients of the two spectra.

Cosine Similarity to Compare Two Spectra

$$\mathrm{Similarity} = \frac{A \cdot B}{||A||||B||} = \frac{\sum_{i=1}^{n} A_i B_i}{\sqrt{\sum_{i=1}^{n} A_i^2}\sqrt{\sum_{i=1}^{n} B_i^2}} \quad (3)$$

https://doi.org/10.1021/acs.jproteome.1c00882
J. Proteome Res. XXXX, XXX, XXX−XXX

IgG Antibody Glycan Analysis

Reduced IgG purified from plasma were separated on an SDS-PAGE gel, and the band corresponding to the heavy chain was cut and subjected to in-gel digestion as follows: gel bands were washed in 100 mM ammonium bicarbonate (AmBic)/acetonitrile (ACN) and reduced with 10 mM dithiothreitol at room temperature for 45 min. Cysteines were alkylated with 50 mM iodoacetamide in the dark for 45 min at room temperature. Finally, gel bands were washed in 100 mM AmBic/ACN prior to adding 600 ng Lys-C for overnight incubation at room temperature. Following digestion, supernatants containing peptides were transferred into new tubes. Gel pieces were washed at room temperature for 10 min with gentle shaking, in 50% ACN/5% FA, and supernatants were combined with peptide solutions. This wash was repeated each by 80% ACN/5% FA, and 100% ACN, and all supernatants was saved. Pooled supernatants were then subject to speedvac drying. After lyophilization, peptides were reconstituted with 5% ACN/0.1% FA in water.

Peptides were analyzed by LC-MS/MS using a Dionex UltiMate 3000 Rapid Separation nanoLC and a Q Exactive HF Hybrid Quadrupole-Orbitrap Mass Spectrometer (Thermo Fisher Scientific Inc.). The peptide samples were loaded onto the trap column, which was 150 μm × 3 cm in-house packed with 3 μm C18 beads. The analytical column was a 75 μm × 10.5 cm PicoChip column packed with 3 μm C18 beads (New Objective). The flow rate was kept at 300 nL/min. Solvent A was 0.1% FA in water and Solvent B was 0.1% FA in ACN. The peptide was separated on a 60 min analytical gradient from 5% to 50% of Solvent B. The mass spectrometer was operated in the Full MS scan. The source voltage was 2.30−2.50 kV and the capillary temperature 320 °C. Full MS scans were acquired from 400 to 2,000 m/z at 60,000 resolving power and automatic gain control (AGC) set to 3×10^6.

MS data were processed using Skyline (ver. 20.2). The integration and correction for the chromatographic peaks of 18 glycans were performed manually. Three of the most intense precursor ions of each glycan were selected, summed, and exported as the quantitative value of the corresponding glycan. Total ion intensities were used to generate the plots.

Plots and Statistical Analysis

IT and DoC-based t-SNE plot was generated on RStudio ver. 1.2.5019 using the Rtsne package and the following parameters: 2 dimensions, perplexity of 7, verbose = true, 1000 maximum interactions, and check_duplicates = False. Mixed effect ANOVA statistics were calculated using SAS (SAS Institute, Cary, NC). Pearson's correlations were calculated using the function "cor.test" and method "pearson" on RStudio ver. 3.1.1073. Violin and dot plots were generated with GraphPad Prism 9.0.2 and that same software was used for calculating the statistical significance by one-way ANOVA with Tukey's multiple comparison test (* $p < 0.05$; ** $p < 0.01$).

Data and Software Availability

Processed data sets utilized for the Ig-MS analyses can be found on the MassiVE repository, MSV000087529. Custom compiled code used to process and create I^{2}MS files is already available.[16] Bottom-up glycan data is available at Panorama Public https://panoramaweb.org/nsRX7w.url. Additional desired software and data that support the findings of this study are available from the corresponding authors upon request.

RESULTS AND DISCUSSION

Benchmarking the Ig-MS Assay

The RBD of the spike protein from SARS-CoV-2 (Wuhan strain) was expressed, purified from HEK293 cells, and characterized by both bottom-up proteomics (100% sequence coverage) and Western blot (Figure S1). Purified RBD was covalently attached to magnetic beads and used as bait for binding and enriching antibodies against SARS-CoV-2-Spike-RBD (Ig-RBD) from the plasma of COVID-19 convalescent individuals (Figure 1A). One hundred nanograms of a standard mAb CR3022 was used as an internal standard in all Ig-MS analyses (see Materials and Methods).

Proof-of-concept experiments used samples derived from a single COVID-19 convalescent individual featuring a high ELISA titer of Ig-RBD, hereafter referred to as CS1 (commercial sample 1). Enrichments from plasma derived from CS1 were performed to optimize parameters such as covalent bead-loading chemistry, the wash, and elution buffer conditions to increase capture and suppress nonspecific binding (see Materials and Methods). As shown in Figure 1B, the optimized pull-down protocol for 100 μL of plasma efficiently captured Ig-RBD, which was isolated with >90% yield in the optimized elution conditions. Pull-downs from CS1 were used to profile the antibody isotypes (IgA, IgD, IgE, and IgM) and IgG subclasses (IgG1, IgG2, IgG3, and IgG4) being enriched. A specific Western blot revealed that IgG1, IgG3, and IgM were the primary isotypes isolated (Figure S2), similar to what has been reported in the literature.[32]

Following antibody enrichment, isolated Ig-RBDs were prepared for Ig-MS analysis (Figure 1A). In the preparation workflow, Ig-RBDs were eluted intact, combined with 100 ng of standard mAb CR3022, and fully reduced/denatured in the presence of a chaotropic agent to liberate HC (48−55 kDa) and LC (22−25 kDa) proteoforms. Finally, the liberated LCs and HCs were precipitated via methanol/chloroform/water, resuspended, and subjected to I^{2}MS acquisition.

To benchmark Ig-MS, we first analyzed mAb CR3022 and annotated the LC and HC proteoforms (Figure S3). Subsequently, we estimated the Ig-MS limit of detection (LOD) for the HC of NIST mAb (with glycosylation) at 100 nM, whereas the LOD for the LC was well below 10 nM (Figure S4). Next, we performed Ig-MS on CS1, and Figure S5 shows the final I^{2}MS spectrum obtained for the LC region and the respective standard m/z spectrum obtained in a regular MS1 experiment. Like in Figure 1C, the highlighted peak at ∼24,268 Da represents the standard mAb CR3022 used to calculate Ig-MS metrics, as outlined in eqs 1−3 in the Materials and Methods. The other peaks with lower mass than the standard LC, ranging from ∼22 to 24 kDa, are distinct LC proteoforms originating from B cell clones with different or isobaric complementarity-determining regions (CDR) sequences in their variable regions. With this first glimpse of an Ig repertoire at the LC and HC levels, the presence of distinct proteoforms shows that single clone resolution is possible, with some present at high titer (i.e., ∼500 ng/100 μL plasma). The current dynamic range for detecting different clones that evolve after VDJ recombination is approximately 100 (Figure S5). This intraspectral dynamic range of 100 is much lower than that previously reported by I^{2}MS analysis. This decrease is due to the large amount of antibody heterogeneity within a small mass domain window. Although the overlap of similar isotopic mass distributions causes mass profiles to appear more

https://doi.org/10.1021/acs.jproteome.1c00882
J. Proteome Res. XXXX, XXX, XXX−XXX

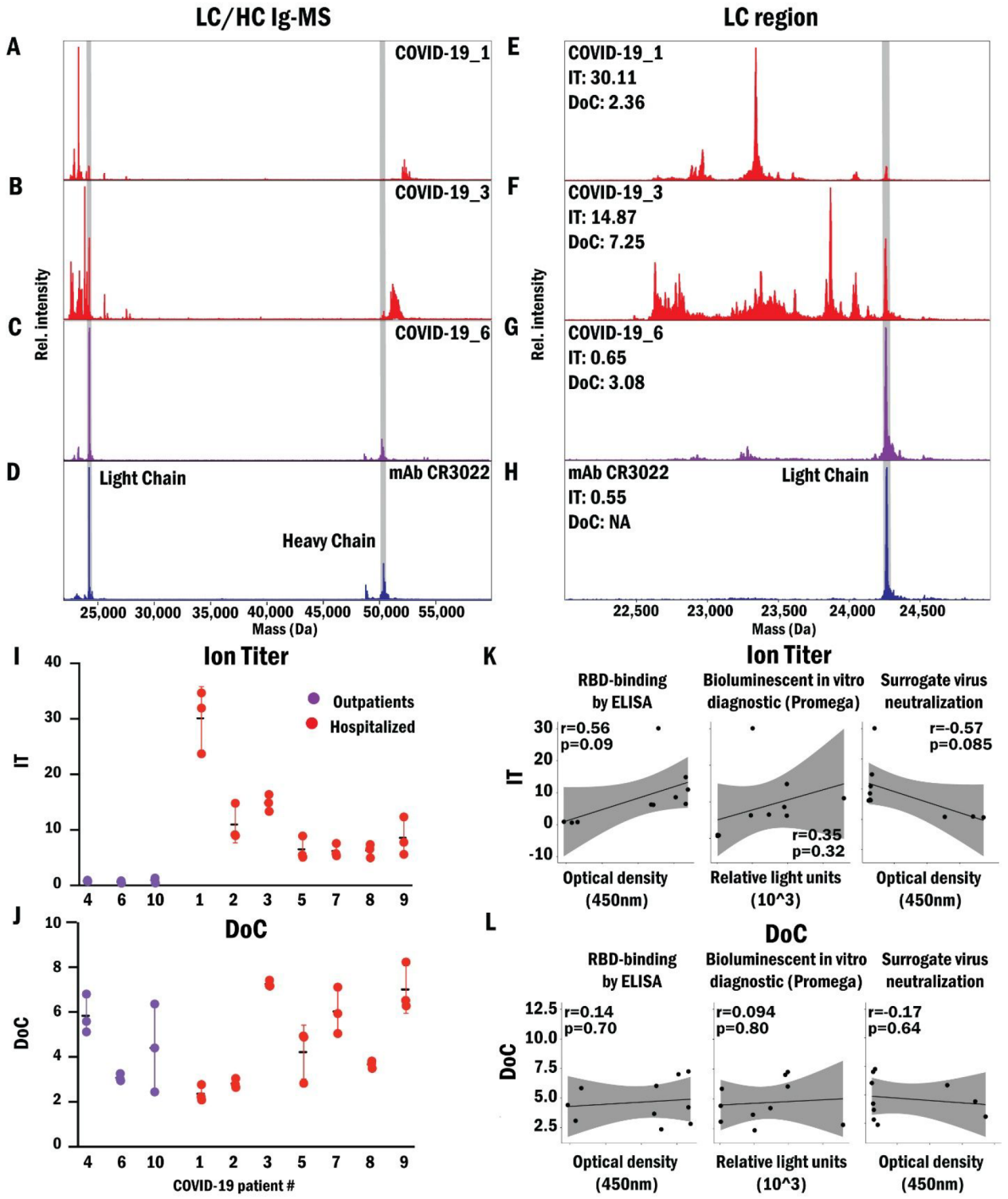

Figure 2. Ig-MS readouts on a COVID-19 cohort. (A–D) LC/HC spectral region and (E–H) expansion of the relative LC region for (A/E and B/F, red) two hospitalized patients and (C/G, purple) one outpatient. The standard mAb (CR3022) (D/H, blue) that binds SARS-CoV-2-RBD was used as a positive control (highlighted with gray vertical bar). (I) Ion titer (IT) and (J) degree of clonality (DoC) values obtained for all three outpatients and seven hospitalized patients. Analyses were done in triplicate. (K) Correlation of IT and (L) DoC values from Ig-MS with RBD-binding by ELISA, bioluminescent in vitro diagnostic (Promega), and surrogate virus neutralization. Shown are the Pearson correlation coefficient (r) and p-value (p).

"noisy" in nature, each signal represented in the I^2MS spectra corresponds to a real antibody species. While more abundant antibody species peek through the complex mass landscape, their relative abundance to an antibody standard gives a view into important information dealing with DoC and IT calculations previously intractable via traditional m/z ensemble ion collection schemes.

https://doi.org/10.1021/acs.jproteome.1c00882
J. Proteome Res. XXXX, XXX, XXX−XXX

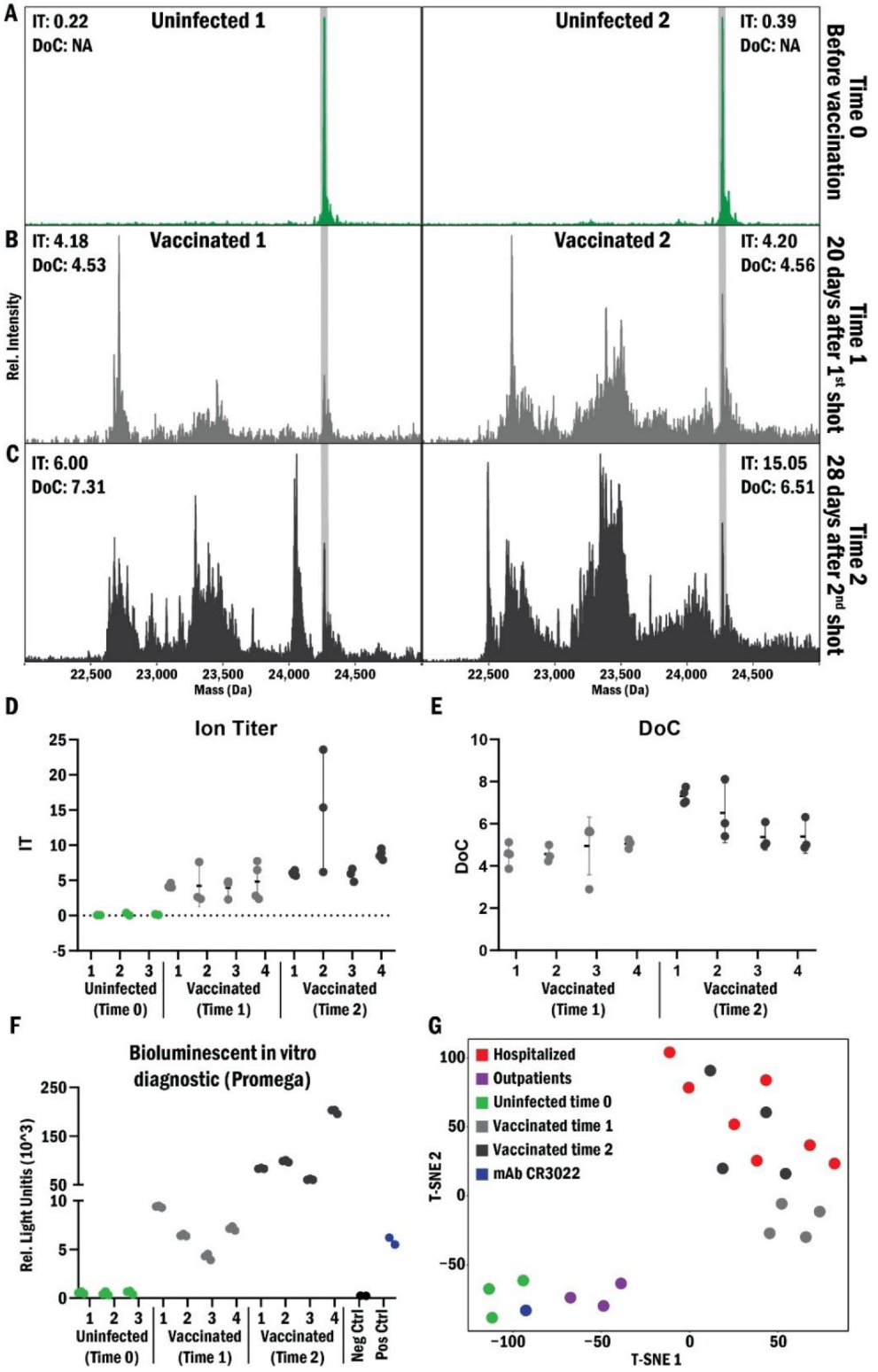

Figure 3. Ig-MS readouts from the vaccinated cohort. LC spectra for (A) uninfected individuals before the vaccination (time 0), (B) vaccinated individuals at 20 days after the first shot (time 1), and (C) at 28 days after the second shot (time 2); spiked-in standard mAb CR3022 highlighted by a gray rectangle. (D) IT and (E) DoC values of Ig-MS for all time points. (F) Bioluminescent in vitro diagnostic (Promega) titer of anti-RBD antibodies. (G) t-SNE plot generated with IT and DoC values from both analyzed cohorts.

Given that Ig-MS produced a new data type, we created two new metrics. The IT is similar to an ELISA titer and uses the intensity of the LC of the standard mAb CR3022 as a reference. It combines intensity of all other LC peaks relative to the mAb CR3022 and ranges from 0 to 100 (eq 1). The second is the DoC, a metric demonstrating the proteoform complexity of an LC spectral region in the mixture. DoC ranges from 1 to infinity, with higher numbers reflecting the presence of a more significant number of antibodies in a more complex Ig-MS spectrum. For subject CS1, the calculated IT

https://doi.org/10.1021/acs.jproteome.1c00882
J. Proteome Res. XXXX, XXX, XXX−XXX

was 1.30, and the DoC was 3.64. We next sought to compare these Ig patterns and new metrics across patients and perform initial correlations with other COVID-19 antibody tests.

Ig-MS of an Initial Cohort

We deployed Ig-MS to survey the Ig population reactive to RBD in a cohort of seven hospitalized patients with severe COVID-19, three outpatients with mild COVID-19 disease, and three uninfected healthy people (Table S1). The standard mAb CR3022 and a commercial pooled serum acquired before November 2019 served as positive and negative controls, respectively. Importantly, the use of serum as control is valid as previous works have established that SARS-CoV-2 antibody measurements and characterization are not influenced by differences in plasma vs serum isolation.[33]

The HC and LC mass distributions obtained by Ig-MS analysis are all shown in Figure S6 for this cohort, while Figures S7 and S8 present expansion of LC and HC regions, respectively. Figure 2A−D highlights HC/LC spectra and Figure 2E−H expansion of LC regions exemplifying three general groups of immunological responses: (**1**) high IT (30.11) and low DoC (2.36) as observed in one of the hospitalized patients (COVID-19_1) (Figure 2A/E); (**2**) moderately high IT (14.87) and high DoC (7.25) as observed for the hospitalized patient COVID-19_3 (Figure 2B/F); and (**3**) low IT (0.65) and low DoC (3.08) as observed for the outpatient COVID-19_6 (Figure 2C/G).

Distinct proteoform masses representing all the LCs were clearly discernible. The LC proteoforms have a mass range between 22 and 25 kDa (Figure 2 E/F/G) and comprise the entire length of the LC, including the three CDRs (VL) and conserved region (CL). We can identify κ and λ LCs in the Ig-MS spectra based on the amino acid differences in the conserved regions. In Figure 2F, the masses between 22.5 and 23 kDa belong to lambda LCs and those from 23 to 24 kDa to kappa LCs.[34] A correlation coefficient (eq 3) was calculated and showed an average value of 0.95 for technical replicates. Figure 2I/J displays the IT and DoC values for all samples from the cohort. The IT values are significantly higher in hospitalized patients (F = 12.64, 2, and 33 DF, $p < 0.001$) compared to outpatients, a result corroborated with standard serological tests from previous studies.[35,36] No statistically significant differences were observed for the DoC metric in these groups.

We next probed the correlation of ITs and DoCs obtained Ig-MS with titers of anti-RBD antibodies quantified with ELISA[37] and a commercial in vitro bioluminescence diagnostic. We also determined their correlation with neutralization efficiency obtained with a spike-specific pseudovirus neutralization test (Figure 2K/L, Figure S9, and Table S1). Pearson's correlation (r) indicated a positive correlation of IT and the ELISA titers ($r > 0.55$) but with p-values higher than 0.05 (Figure 2K). Furthermore, DoCs did not correlate with the other assays (Figure 2L), indicating that the number of different Ig signals produced by Ig-MS did not show a correlation with neutralization potential or overall titer in this initial study.

Ig-MS of a Vaccinated Cohort

To compare natural infection with vaccination, we used Ig-MS to analyze plasma from uninfected subjects (time 0) that were immunized with the BNT162b2 vaccine from Pfizer and BioNTech. Specifically, we analyzed the same subjects at 20 days after the first shot (time 1) and 28 days after the second shot (time 2).

Focusing only on the LC proteoform repertoire, at time 0 the Ig-MS spectrum for the uninfected subjects shows only the LC of the standard mAb CR3022 (Figure 3A and Figure S10), indicating the absence of patient-derived antibodies that recognize SARS-CoV-2 RBD. After the first vaccine shot (time 1), the emergence of several anti-RBD antibodies were observed (Figure 3B and Figure S10). After the second shot (time 2), there were substantial increases in the titer (IT) and complexity (DoC) of anti-RBD antibodies (Figure 3C and Figure S10). The increase of IT following the two vaccine doses (Figure 3D) was statistically significant for times 1 to 2 (p-value 0.006) and 0 to 2 (p-value 0.00005), but not for time 0 to 1 (p-value 0.06) using a mixed model ANOVA testing the effect of the three time points while allowing individual subjects to have independent means. All p-values were Bonferroni corrected for multiple testing. Additionally, the DoC increase is also statistically significant comparing times 1 and 2 (p-value 0.002) for all individuals (Figure 3E), representing the emergence of new LC proteoforms after the second vaccine shot. Importantly, the IT results calculated with Ig-MS are in accordance with what was observed using more traditional titer assays, including the bioluminescent in vitro diagnostic from Promega (Figure 3F) and ELISA (Table S1).

We also observed changes in the distribution and intensities of the individual LC proteoforms. For example, the most abundant LC antibody at time 1 for the vaccinated 1 subject has a mass of ∼22,700 Da and an intensity three times higher than the standard mAb CR3022 (Figure 3B left panel). At time 2 for the same individual, the most abundant LC proteoform has a mass of ∼24,050 Da with an abundance approximately two times higher than the mAb CR3022, and the LC at ∼22,700 Da is only the fifth most abundant peak (Figure 3C left panel) at this time. Such detection capability makes Ig-MS the only method available that captures the longitudinal dynamics of a subject's antibody repertoire with single clone resolution.

Finally, we used the IT and DoC values obtained from Ig-MS to generate a t-SNE plot representing the antibody responses of all analyzed subjects, including both the vaccinated and infected cohorts. Figure 3G shows that uninfected individuals cluster close to the COVID-19 outpatients, and this cluster is far from the major cluster formed by COVID-19 hospitalized and vaccinated individuals. Furthermore, vaccinated individuals after the first dose (time 1) cluster together and are differentiated from the severe COVID-19 patients and individuals after the vaccine boost (time 2). These results show that after the second dose of the vaccine, the antibody response measured by IT and DoC is comparable to the one generated in COVID-19 hospitalized individuals. Importantly, even one dose of the vaccine generates a more robust immune response than the one observed in COVID-19 outpatients.

Reducing HC Complexity Using IdeS

LC/HC Ig-MS analysis focuses almost exclusively on LC proteoforms. Our early observation was that intact HC has a higher LOD, highly complex distributions, with more overlapping isotopic distributions. Such complexity results from highly variable glycosylation explicitly localized to the Fc domain of the HC that modulates antibody effector function.

https://doi.org/10.1021/acs.jproteome.1c00882
J. Proteome Res. XXXX, XXX, XXX−XXX

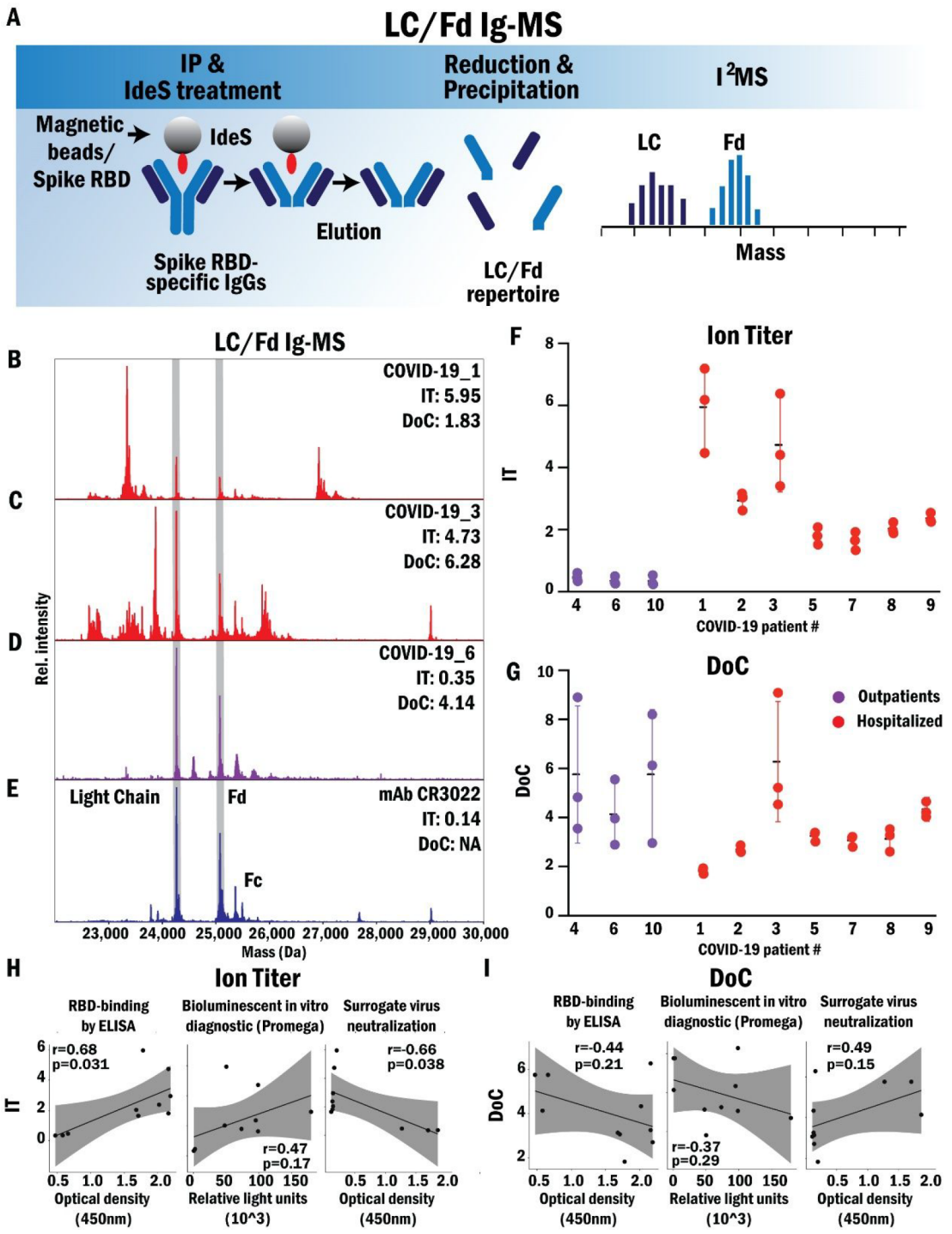

Figure 4. LC/Fd Ig-MS readouts on the COVID-19 cohort. (A) Overview of sample preparation and readout for LC/Fd Ig-MS. Antibodies against RBD are enriched from the plasma/serum of COVID-19 patients or control uninfected individuals with magnetic beads conjugated with RBD protein. Before elution, RBD-specific Igs are digested with the IdeS enzyme to remove the Fc domain of the HC. The eluates are then reduced to liberate LC and Fd, which are analyzed by I^2MS. (B–E) LC/Fd spectral region for (B/C, red) two hospitalized patients and (D, purple) one outpatient. The standard mAb (CR3022) (E, blue) that binds SARS-CoV-2-RBD was used as a positive control (highlighted with gray vertical bar). (F) Ion titer (IT) and (G) degree of clonality (DoC) values were obtained for three outpatients and seven hospitalized patients. Analyses were done in triplicate. (H) Correlation of IT and (I) DoC values with RBD-binding by ELISA, bioluminescent in vitro diagnostic (Promega), and surrogate virus neutralization. Shown are the Pearson correlation coefficient (r) and p-value (p).

To better capture the sequence variation of the HC, we developed a second Ig-MS workflow that generates LC and the Fd domain of the HC via a proteolytic digest step (Figure 4A). Here, after interaction with the RBD, patient Ig-RBD is digested with IdeS protease while still attached to the beads, generating $F(ab')_2$ and Fc. The protease and Fc species (containing HC glycosylation) are entirely washed away. Eluted $F(ab')_2$ are denatured and reduced to yield the LC and the Fd domain (~25–28 kDa), which contains the N-terminal 220 amino acids of the HC, before I^2MS analysis. With LC/Fd

https://doi.org/10.1021/acs.jproteome.1c00882
J. Proteome Res. XXXX, XXX, XXX−XXX

Ig-MS, we can analyze Fd proteoforms that include three CDRs from the HC (VH) and the constant region CH1.

We repeated Ig-MS analysis of the patient cohort presented previously, this time using LC/Fd Ig-MS. Figure S11 exhibits the obtained spectra for all samples. The spectra from patients COVID-19_1 (Figure 4B), COVID-19_3 (Figure 4C), and COVID-19_6 (Figure 4D) displayed the same immunological response pattern as those obtained with LC/HC Ig-MS, showing the self-consistency of the two workflows. Additionally, the same basic patterns of LC proteoforms were observed with both workflows applied to the same sample. For example, a comparison of LC proteoform patterns for patient COVID-19_3 showed a correlation coefficient of 0.77 (Figure S12). As previously observed, IT values were statistically significantly higher for hospitalized patients (F = 18.26, 2, and 33 DF, p < 0.001; Figure 4F) and there was no difference in the DoC for the two groups (Figure 4G). A comparison of ITs calculated for LC regions using both workflows revealed that despite some differences in the range of ITs, there was a strong correlation (R^2 = 0.88) between them, indicating a systematic bias (Figure S12). We believe that this bias arises from the differences in sample and standard preparation. However, the average cross-correlation of the LC from the two studies is 0.78 ± 0.04, indicating that the ratios among peaks and the relative proteoform amounts are conserved.

The ITs significantly correlate with ELISA titers (r = 0.68) and the neutralization efficiency (r = −0.66) (Figure 4H). As observed before, the correlation of ITs with the bioluminescence was also low ($r \leq 0.47$) and not significant. In addition, DoCs did not correlate with any of the other assays (Figure 4I). Interestingly, both for LC/HC and LC/Fd Ig-MS, there was a significant negative correlation between ITs and days after infection, but not for DoC (Figure S13). These results suggest that there is a reduction in the total amount of antibodies over time, but the general degree of complexity in the immune response does not change. Additionally, virus neutralization appears more related to the total amount of antibodies in the plasma than to clonal heterogeneity in the Ig repertoire.

IgG Glycosylation Analysis

N-glycosylation at position 297 of the HC mediates the antibody's effector functions. Further, the glycan moieties are highly variable and functionally relevant. To explore the IgG glycosylation pattern of our three study groups, we used bottom-up proteomics to quantify 17 different glycan structures (attached to the IgG peptide) using Skyline[38] and the unmodified peptide.[39] A Benjamini and Hochberg corrected ANOVA analysis on the results from the three groups indicated that seven fucosylated glycans (G2F, G0FN, G1FN, G2FN, G1FS1, G2FS1, and G2FS2) were differentially regulated. A second one-way ANOVA with Tukey's multiple comparison test revealed that those fucosylated glycans were down-regulated in the hospitalized group compared to the uninfected group (Figure S14).

Additionally, the average percent of the total fucosylated glycans was 53.9% ± 17.7% for the hospitalized group and 95.5% ± 0.8% for the uninfected individuals (Figure S15). Similar results were previously reported,[40] and afucosylated IgG induces antibody-dependent cellular cytotoxicity by increasing IgG-Fc receptor IIIa (FcγRIIIa) affinity.[41] Next, we tried to correlate these results to the LC/HC Ig-MS readouts. Unfortunately, the high mass complexity observed in the HC region of workflow 1 generated from the different amino acid sequences and the multiple glycans structures pushes such analyses outside the scope of this initial study.

Ig-MS in Context

Antibody titers can be used to indicate the extent of immunity and severity for diseases such as COVID-19.[35,36] Ig-MS initial results showed that IT calculated from LC spectra of LC/HC and LC/Fd Ig-MS were self-consistent and correlated with traditional colorimetric/fluorimetric tests and a surrogate neutralization assay. The DoC metric and patterns of responses did not correlate with these assays, yet their variance in the human population needs to be determined. We observed significant differences in hospitalized patients versus outpatients as well as reduced IT over time of convalescence, similar to previous reports.[42] Vaccinated individuals featured an increase in antibody intensity and clonal complexity detected by significant IT and DoC rise over time. Preceding reports[43,44] showed an increase in antibody amounts and neutralization capacity, but this is the first time we can resolve and visualize the surge in antibody proteoform diversity at the protein level. Additionally, fully vaccinated individuals had a similar immune response to hospitalized patients. This initial report demonstrates the functionality of Ig-MS, and prompts three general use cases for this approach: (1) providing a new longitudinally stable, multiparametric correlate of protection for vaccinated and recovered individuals; (2) indicating the course or stage of COVID-19 disease as a diagnostic or prognostic indicator; and (3) striating lots of convalescent plasma to quantify protective potential and better control plasma collection campaigns in this or future pandemics.[45] Moreover, antibody amounts and clonal variation can play a complementary role in vaccine campaigns.

Ig-MS Future Directions

Reports in the literature have begun to quantify the extent of convergence in the sequences of antibodies by deep sequencing of B cell receptors.[46,47] These reports quantified responses across over 100 people and thousands of B cells, demonstrating the consistency of the stereotypical immune response, and are a great resource to identify potential therapeutic and prophylactic antibodies. Such convergence can also be detected by Ig-MS because it provides intact mass patterns that reflect the combination of LC and HC CDRs. This is unlike approaches using tryptic digestion of antibodies.[8−11,48] Indeed, no technology can sequence whole, endogenous antibodies directly in an Ig repertoire, but >80% sequence coverage by direct fragmentation of LC and HC from monoclonal antibodies is possible today.[49]

Moving forward, we will expand the cohort sizes of recovered and vaccinated studies into the hundreds to define correlations with subjects to clinical metadata and other assays. Importantly, Ig-MS is easily adaptable to other targets by simply changing the bait antigen loaded onto the affinity resin, enabling the use of the approach to investigate RBD Spike proteins from SARS-CoV-2 variant strains (e.g., Beta and Delta) to probe vaccination effectiveness and establish Ig-MS utility as a new correlate of protection in serology. In addition, there are reports of neutralizing epitopes in the N-terminal domain (NTD) of Spike, and we can further probe this to elucidate antibody repertoires.[50] Analysis of longitudinal samples from individuals infected with SARS-CoV-2 and after vaccination will track the immune response at high resolution.[42,51] Ig-MS should also be applicable to IgAs, IgMs,

https://doi.org/10.1021/acs.jproteome.1c00882
J. Proteome Res. XXXX, XXX, XXX−XXX

and other isotypes of immunoglobulins in the adaptive immune response.

CONCLUSIONS

In summary, we report a new and unique data type for human serology, using COVID-19 cases and vaccinated individuals as the first examples. Until now, no serological test was capable of accessing the relative abundance of each antibody generated against a specific antigen. Ig-MS is the first method capable of accessing amounts and relative abundance of antibodies simultaneously using a fundamental advance in MS of individual protein ions[16] to create a unique display of the Ig repertoire of a human being at molecular resolution. Ig-MS successfully captured the clone populations of RBD-reactive immunoglobulins and showed promising data on a limited cohort of COVID-19 patients and vaccinated subjects. In the future, a more automated form of Ig-MS will address larger cohorts, use 10−100-fold less sample, and extensively sequence CDR variable regions for comparison with methods for single B cell sequencing like Ig-seq.[52]

ASSOCIATED CONTENT

Supporting Information

The Supporting Information is available free of charge at https://pubs.acs.org/doi/10.1021/acs.jproteome.1c00882.

Additional experimental results, including I^{2}MS spectra, charts, Western blots, and a summary table with multiple assay results. Figure S1: Expression validation of RBD region from the SARS-CoV-2 Spike protein; Figure S2: Western blot showing isotypes and IgG subclasses of the antibodies enriched with Ig-MS assay; Figure S3: Proteoform annotation of the CR3022 standard monoclonal antibody; Figure S4: Titration curve for Ig-MS to estimate the limit of detection (LOD) for NIST standard monoclonal antibody; Figure S5: Ig-MS readout of light chain region for CS1; Figure S6: Ig-MS readouts for Light and Heavy Chains; Figure S7: Ig-MS readouts of Light Chains; Figure S8: Ig-MS readouts of Heavy Chains; Figure S9: Anti-RBD antibody and neutralization titers, Figure S10: Ig-MS readouts from the vaccinated cohort; Figure S11: Ig-MS readouts of Light Chain and Fd domain; Figure S12: Comparison of ion titers between LC/HC and LC/Fd Ig-MS. Figure S13: Correlation of Ion titer (IT) and Degree of Clonality (DoC) metrics from Ig-MS with days after infection; Figure S14: Comparison of bulk IgG glycosylation profiles; Figure S15: Comparison of total glycan composition; Table S1: Correlation of Ig-MS metrics with patient metadata (PDF)

AUTHOR INFORMATION

Corresponding Author

Neil L. Kelleher − *Departments of Molecular Biosciences, Chemistry, Northwestern University, Evanston, Illinois 60208, United States; Proteomics Center of Excellence, Evanston, Illinois 60208, United States; Department of Biochemistry and Molecular Genetics, Northwestern University Feinberg School of Medicine, Chicago, Illinois 60611, United States;* orcid.org/0000-0002-8815-3372; Email: n-kelleher@northwestern.edu

Authors

Rafael D. Melani − *Departments of Molecular Biosciences, Chemistry, Northwestern University, Evanston, Illinois 60208, United States;* orcid.org/0000-0002-0349-235X

Benjamin J. Des Soye − *Departments of Molecular Biosciences, Chemistry, Northwestern University, Evanston, Illinois 60208, United States; Proteomics Center of Excellence, Evanston, Illinois 60208, United States*

Jared O. Kafader − *Departments of Molecular Biosciences, Chemistry, Northwestern University, Evanston, Illinois 60208, United States;* orcid.org/0000-0002-5359-264X

Eleonora Forte − *Proteomics Center of Excellence, Evanston, Illinois 60208, United States; Department of Surgery, Feinberg School of Medicine, Northwestern University, Chicago, Illinois 60611, United States*

Michael Hollas − *Departments of Molecular Biosciences, Chemistry, Northwestern University, Evanston, Illinois 60208, United States;* orcid.org/0000-0002-0797-3134

Voislav Blagojevic − *Departments of Molecular Biosciences, Chemistry, Northwestern University, Evanston, Illinois 60208, United States*

Fernanda Negrão − *Departments of Molecular Biosciences, Chemistry, Northwestern University, Evanston, Illinois 60208, United States*

John P. McGee − *Departments of Molecular Biosciences, Chemistry, Northwestern University, Evanston, Illinois 60208, United States*

Bryon Drown − *Departments of Molecular Biosciences, Chemistry, Northwestern University, Evanston, Illinois 60208, United States*

Cameron Lloyd-Jones − *Departments of Molecular Biosciences, Chemistry, Northwestern University, Evanston, Illinois 60208, United States*

Henrique S. Seckler − *Departments of Molecular Biosciences, Chemistry, Northwestern University, Evanston, Illinois 60208, United States;* orcid.org/0000-0001-8989-5303

Jeannie M. Camarillo − *Departments of Molecular Biosciences, Chemistry, Northwestern University, Evanston, Illinois 60208, United States*

Philip D. Compton − *Departments of Molecular Biosciences, Chemistry, Northwestern University, Evanston, Illinois 60208, United States; Integrated Protein Technologies, Evanston, Illinois 60201, United States*

Richard D. LeDuc − *Departments of Molecular Biosciences, Chemistry, Northwestern University, Evanston, Illinois 60208, United States;* orcid.org/0000-0002-6951-2923

Bryan Early − *Departments of Molecular Biosciences, Chemistry, Northwestern University, Evanston, Illinois 60208, United States*

Ryan T. Fellers − *Departments of Molecular Biosciences, Chemistry, Northwestern University, Evanston, Illinois 60208, United States*

Byoung-Kyu Cho − *Proteomics Center of Excellence, Evanston, Illinois 60208, United States*

Basil Baby Mattamana − *Proteomics Center of Excellence, Evanston, Illinois 60208, United States*

Young Ah Goo − *Departments of Molecular Biosciences, Chemistry, Northwestern University, Evanston, Illinois 60208, United States; Proteomics Center of Excellence, Evanston, Illinois 60208, United States*

Paul M. Thomas − *Departments of Molecular Biosciences, Chemistry, Northwestern University, Evanston, Illinois*

https://doi.org/10.1021/acs.jproteome.1c00882
J. Proteome Res. XXXX, XXX, XXX−XXX

60208, United States; Proteomics Center of Excellence, Evanston, Illinois 60208, United States

Michelle K. Ash − *Department of Microbial Pathogens and Immunity, Rush University Medical Center, Chicago, Illinois 60612, United States*

Pavan P. Bhimalli − *Department of Microbial Pathogens and Immunity, Rush University Medical Center, Chicago, Illinois 60612, United States*

Lena Al-Harthi − *Department of Microbial Pathogens and Immunity, Rush University Medical Center, Chicago, Illinois 60612, United States*

Beverly E. Sha − *Division of Infectious Diseases, Rush University Medical Center, Chicago, Illinois 60612, United States*

Jeffrey R. Schneider − *Department of Microbial Pathogens and Immunity, Rush University Medical Center, Chicago, Illinois 60612, United States*

Complete contact information is available at: https://pubs.acs.org/10.1021/acs.jproteome.1c00882

Author Contributions

▲R.D.M., B.J.D., J.O.K., and E.F. contributed equally to this work.

Notes

The authors declare the following competing financial interest(s): N.L.K., J.O.K., and P.D.C. report a conflict of interest with I^2MS technology used to readout the Ig profiles, currently being commercialized by Thermo Fisher Scientific.

■ ACKNOWLEDGMENTS

RBD was expressed by the Northwestern Recombinant Protein Production Core Facility. The reagent was produced under HHSN272201400008C and obtained through BEI Resources, NIAID, NIH: Vector pCAGGS Containing the SARS-Related Coronavirus 2, Wuhan-Hu-1 Spike Glycoprotein Receptor-Binding Domain (RBD), NR-52309. IgG glycosylation and bottom-up proteomics were measured by the Northwestern Proteomics Core Facility. This study was funded by the National Institute of Health under a grant from the National Institute of General Medical Sciences P41 GM108569 (N.L.K.); the Research Corporation (Grant no. 27372, N.L.K. and E.F.); Administrative Supplement to SBIR grant number R44 GM121130 (P.D.C.); Walder Foundation grant number SCI16 (J.R.S.); the NIH Office of Director award S10 OD025194 (P.D.C.); the Northwestern Medicine Dr. Michael M. Abecassis Transplant Innovation Endowment Grant; NCI CCSG P30 CA060553 (awarded to the Robert H. Lurie Comprehensive Cancer Center). National Cancer Institute grant 1F32CA246894-01A1 (B.D.); The content of this paper is solely the responsibility of the authors and does not necessarily represent the official views of the National Institutes of Health.

■ REFERENCES

(1) Zhou, P.; Yang, X. L.; Wang, X. G.; Hu, B.; Zhang, L.; Zhang, W.; Si, H. R.; Zhu, Y.; Li, B.; Huang, C. L.; Chen, H. D.; Chen, J.; Luo, Y.; Guo, H.; Jiang, R. D.; Liu, M. Q.; Chen, Y.; Shen, X. R.; Wang, X.; Zheng, X. S.; Zhao, K.; Chen, Q. J.; Deng, F.; Liu, L. L.; Yan, B.; Zhan, F. X.; Wang, Y. Y.; Xiao, G. F.; Shi, Z. L. A pneumonia outbreak associated with a new coronavirus of probable bat origin. *Nature* **2020**, *579* (7798), 270−273.

(2) Zhou, Y.; Yang, Q.; Chi, J.; Dong, B.; Lv, W.; Shen, L.; Wang, Y. Comorbidities and the risk of severe or fatal outcomes associated with coronavirus disease 2019: A systematic review and meta-analysis. *Int. J. Infect. Dis.* **2020**, *99*, 47−56.

(3) Ahmad, F. B.; Cisewski, J. A.; Minino, A.; Anderson, R. N. Provisional Mortality Data - United States, 2020. *MMWR Morb Mortal Wkly Rep* **2021**, *70* (14), 519−522.

(4) Wang, P.; Nair, M. S.; Liu, L.; Iketani, S.; Luo, Y.; Guo, Y.; Wang, M.; Yu, J.; Zhang, B.; Kwong, P. D.; Graham, B. S.; Mascola, J. R.; Chang, J. Y.; Yin, M. T.; Sobieszczyk, M.; Kyratsous, C. A.; Shapiro, L.; Sheng, Z.; Huang, Y.; Ho, D. D. Antibody resistance of SARS-CoV-2 variants B.1.351 and B.1.1.7. *Nature* **2021**, *593*, 130−135.

(5) Wu, J.; Liang, B.; Chen, C.; Wang, H.; Fang, Y.; Shen, S.; Yang, X.; Wang, B.; Chen, L.; Chen, Q.; Wu, Y.; Liu, J.; Yang, X.; Li, W.; Zhu, B.; Zhou, W.; Wang, H.; Li, S.; Lu, S.; Liu, D.; Li, H.; Krawczyk, A.; Lu, M.; Yang, D.; Deng, F.; Dittmer, U.; Trilling, M.; Zheng, X. SARS-CoV-2 infection induces sustained humoral immune responses in convalescent patients following symptomatic COVID-19. *Nat. Commun.* **2021**, *12* (1), 1813.

(6) Kreer, C.; Zehner, M.; Weber, T.; Ercanoglu, M. S.; Gieselmann, L.; Rohde, C.; Halwe, S.; Korenkov, M.; Schommers, P.; Vanshylla, K.; Di Cristanziano, V.; Janicki, H.; Brinker, R.; Ashurov, A.; Krahling, V.; Kupke, A.; Cohen-Dvashi, H.; Koch, M.; Eckert, J. M.; Lederer, S.; Pfeifer, N.; Wolf, T.; Vehreschild, M.; Wendtner, C.; Diskin, R.; Gruell, H.; Becker, S.; Klein, F. Longitudinal Isolation of Potent Near-Germline SARS-CoV-2-Neutralizing Antibodies from COVID-19 Patients. *Cell* **2020**, *182* (6), 1663−1673.

(7) Rogers, T. F.; Zhao, F.; Huang, D.; Beutler, N.; Burns, A.; He, W. T.; Limbo, O.; Smith, C.; Song, G.; Woehl, J.; Yang, L.; Abbott, R. K.; Callaghan, S.; Garcia, E.; Hurtado, J.; Parren, M.; Peng, L.; Ramirez, S.; Ricketts, J.; Ricciardi, M. J.; Rawlings, S. A.; Wu, N. C.; Yuan, M.; Smith, D. M.; Nemazee, D.; Teijaro, J. R.; Voss, J. E.; Wilson, I. A.; Andrabi, R.; Briney, B.; Landais, E.; Sok, D.; Jardine, J. G.; Burton, D. R. Isolation of potent SARS-CoV-2 neutralizing antibodies and protection from disease in a small animal model. *Science* **2020**, *369* (6506), 956−963.

(8) Wine, Y.; Boutz, D. R.; Lavinder, J. J.; Miklos, A. E.; Hughes, R. A.; Hoi, K. H.; Jung, S. T.; Horton, A. P.; Murrin, E. M.; Ellington, A. D.; Marcotte, E. M.; Georgiou, G. Molecular deconvolution of the monoclonal antibodies that comprise the polyclonal serum response. *Proc. Natl. Acad. Sci. U. S. A.* **2013**, *110* (8), 2993−8.

(9) Georgiou, G.; Ippolito, G. C.; Beausang, J.; Busse, C. E.; Wardemann, H.; Quake, S. R. The promise and challenge of high-throughput sequencing of the antibody repertoire. *Nat. Biotechnol.* **2014**, *32* (2), 158−68.

(10) Cheung, W. C.; Beausoleil, S. A.; Zhang, X.; Sato, S.; Schieferl, S. M.; Wieler, J. S.; Beaudet, J. G.; Ramenani, R. K.; Popova, L.; Comb, M. J.; Rush, J.; Polakiewicz, R. D. A proteomics approach for the identification and cloning of monoclonal antibodies from serum. *Nat. Biotechnol.* **2012**, *30* (5), 447−52.

(11) Tran, N. H.; Rahman, M. Z.; He, L.; Xin, L.; Shan, B.; Li, M. Complete De Novo Assembly of Monoclonal Antibody Sequences. *Sci. Rep.* **2016**, *6*, 31730.

(12) Wheatley, A. K.; Juno, J. A.; Wang, J. J.; Selva, K. J.; Reynaldi, A.; Tan, H. X.; Lee, W. S.; Wragg, K. M.; Kelly, H. G.; Esterbauer, R.; Davis, S. K.; Kent, H. E.; Mordant, F. L.; Schlub, T. E.; Gordon, D. L.; Khoury, D. S.; Subbarao, K.; Cromer, D.; Gordon, T. P.; Chung, A. W.; Davenport, M. P.; Kent, S. J. Evolution of immune responses to SARS-CoV-2 in mild-moderate COVID-19. *Nat. Commun.* **2021**, *12* (1), 1162.

(13) Lee, J.; Boutz, D. R.; Chromikova, V.; Joyce, M. G.; Vollmers, C.; Leung, K.; Horton, A. P.; DeKosky, B. J.; Lee, C. H.; Lavinder, J. J.; Murrin, E. M.; Chrysostomou, C.; Hoi, K. H.; Tsybovsky, Y.; Thomas, P. V.; Druz, A.; Zhang, B.; Zhang, Y.; Wang, L.; Kong, W. P.; Park, D.; Popova, L. I.; Dekker, C. L.; Davis, M. M.; Carter, C. E.; Ross, T. M.; Ellington, A. D.; Wilson, P. C.; Marcotte, E. M.; Mascola, J. R.; Ippolito, G. C.; Krammer, F.; Quake, S. R.; Kwong, P. D.; Georgiou, G. Molecular-level analysis of the serum antibody

repertoire in young adults before and after seasonal influenza vaccination. *Nat. Med.* **2016**, *22* (12), 1456−1464.
(14) Smith, L. M.; Kelleher, N. L. Proteoform: a single term describing protein complexity. *Nat. Methods* **2013**, *10* (3), 186−7.
(15) He, L.; Anderson, L. C.; Barnidge, D. R.; Murray, D. L.; Hendrickson, C. L.; Marshall, A. G. Analysis of Monoclonal Antibodies in Human Serum as a Model for Clinical Monoclonal Gammopathy by Use of 21 T FT-ICR Top-Down and Middle-Down MS/MS. *J. Am. Soc. Mass Spectrom.* **2017**, *28* (5), 827−838.
(16) Kafader, J. O.; Melani, R. D.; Durbin, K. R.; Ikwuagwu, B.; Early, B. P.; Fellers, R. T.; Beu, S. C.; Zabrouskov, V.; Makarov, A. A.; Maze, J. T.; Shinholt, D. L.; Yip, P. F.; Tullman-Ercek, D.; Senko, M. W.; Compton, P. D.; Kelleher, N. L. Multiplexed mass spectrometry of individual ions improves measurement of proteoforms and their complexes. *Nat. Methods* **2020**, *17* (4), 391−394.
(17) Schachner, L. F.; Jooss, K.; Morgan, M. A.; Piunti, A.; Meiners, M. J.; Kafader, J. O.; Lee, A. S.; Iwanaszko, M.; Cheek, M. A.; Burg, J. M.; Howard, S. A.; Keogh, M. C.; Shilatifard, A.; Kelleher, N. L. Decoding the protein composition of whole nucleosomes with Nuc-MS. *Nat. Methods* **2021**, *18* (3), 303−308.
(18) Kafader, J. O.; Durbin, K. R.; Melani, R. D.; Des Soye, B. J.; Schachner, L. F.; Senko, M. W.; Compton, P. D.; Kelleher, N. L. Individual Ion Mass Spectrometry Enhances the Sensitivity and Sequence Coverage of Top-Down Mass Spectrometry. *J. Proteome Res.* **2020**, *19* (3), 1346−1350.
(19) Kafader, J. O.; Melani, R. D.; Schachner, L. F.; Ives, A. N.; Patrie, S. M.; Kelleher, N. L.; Compton, P. D. Native vs Denatured: An in Depth Investigation of Charge State and Isotope Distributions. *J. Am. Soc. Mass Spectrom.* **2020**, *31* (3), 574−581.
(20) Kafader, J. O.; Melani, R. D.; Senko, M. W.; Makarov, A. A.; Kelleher, N. L.; Compton, P. D. Measurement of Individual Ions Sharply Increases the Resolution of Orbitrap Mass Spectra of Proteins. *Anal. Chem.* **2019**, *91* (4), 2776−2783.
(21) McGee, J. P.; Melani, R. D.; Yip, P. F.; Senko, M. W.; Compton, P. D.; Kafader, J. O.; Kelleher, N. L. Isotopic Resolution of Protein Complexes up to 466 kDa Using Individual Ion Mass Spectrometry. *Anal. Chem.* **2021**, *93* (5), 2723−2727.
(22) Stadlbauer, D.; Amanat, F.; Chromikova, V.; Jiang, K.; Strohmeier, S.; Arunkumar, G. A.; Tan, J.; Bhavsar, D.; Capuano, C.; Kirkpatrick, E.; Meade, P.; Brito, R. N.; Teo, C.; McMahon, M.; Simon, V.; Krammer, F. SARS-CoV-2 Seroconversion in Humans: A Detailed Protocol for a Serological Assay, Antigen Production, and Test Setup. *Curr. Protoc Microbiol* **2020**, *57* (1), No. e100.
(23) Toby, T. K.; Fornelli, L.; Srzentic, K.; DeHart, C. J.; Levitsky, J.; Friedewald, J.; Kelleher, N. L. A comprehensive pipeline for translational top-down proteomics from a single blood draw. *Nat. Protoc.* **2019**, *14* (1), 119−152.
(24) Wessel, D.; Flugge, U. I. A method for the quantitative recovery of protein in dilute solution in the presence of detergents and lipids. *Anal. Biochem.* **1984**, *138* (1), 141−3.
(25) Skinner, O. S.; Havugimana, P. C.; Haverland, N. A.; Fornelli, L.; Early, B. P.; Greer, J. B.; Fellers, R. T.; Durbin, K. R.; Do Vale, L. H.; Melani, R. D.; Seckler, H. S.; Nelp, M. T.; Belov, M. E.; Horning, S. R.; Makarov, A. A.; LeDuc, R. D.; Bandarian, V.; Compton, P. D.; Kelleher, N. L. An informatic framework for decoding protein complexes by top-down mass spectrometry. *Nat. Methods* **2016**, *13* (3), 237−40.
(26) Park, H.-M.; Winton, V. J.; Drader, J. J.; Manalili Wheeler, S.; Lazar, G. A.; Kelleher, N. L.; Liu, Y.; Tran, J. C.; Compton, P. D. Novel Interface for High-Throughput Analysis of Biotherapeutics by Electrospray Mass Spectrometry. *Anal. Chem.* **2020**, *92* (2), 2186−2193.
(27) Kafader, J. O.; Durbin, K. R.; Melani, R. D.; Des Soye, B. J.; Schachner, L. F.; Senko, M. W.; Compton, P. D.; Kelleher, N. L. Individual Ion Mass Spectrometry Enhances the Sensitivity and Sequence Coverage of Top-Down Mass Spectrometry. *J. Proteome Res.* **2020**, *19* (3), 1346−1350.
(28) McGee, J. P.; Melani, R. D.; Yip, P. F.; Senko, M. W.; Compton, P. D.; Kafader, J. O.; Kelleher, N. L. Isotopic Resolution of Protein Complexes up to 466 kDa Using Individual Ion Mass Spectrometry. *Anal. Chem.* **2021**, *93* (5), 2723−2727.
(29) Kafader, J. O.; Beu, S. C.; Early, B. P.; Melani, R. D.; Durbin, K. R.; Zabrouskov, V.; Makarov, A. A.; Maze, J. T.; Shinholt, D. L.; Yip, P. F.; Kelleher, N. L.; Compton, P. D.; Senko, M. W. STORI Plots Enable Accurate Tracking of Individual Ion Signals. *J. Am. Soc. Mass Spectrom.* **2019**, *30* (11), 2200−2203.
(30) Horn, D. M.; Zubarev, R. A.; McLafferty, F. W. Automated reduction and interpretation of high resolution electrospray mass spectra of large molecules. *J. Am. Soc. Mass Spectrom.* **2000**, *11* (4), 320−32.
(31) Senko, M. W.; Beu, S. C.; McLafferty, F. W. Determination of monoisotopic masses and ion populations for large biomolecules from resolved isotopic distributions. *J. Am. Soc. Mass Spectrom.* **1995**, *6* (4), 229−233.
(32) Amanat, F.; Stadlbauer, D.; Strohmeier, S.; Nguyen, T. H. O.; Chromikova, V.; McMahon, M.; Jiang, K.; Arunkumar, G. A.; Jurczyszak, D.; Polanco, J.; Bermudez-Gonzalez, M.; Kleiner, G.; Aydillo, T.; Miorin, L.; Fierer, D. S.; Lugo, L. A.; Kojic, E. M.; Stoever, J.; Liu, S. T. H.; Cunningham-Rundles, C.; Felgner, P. L.; Moran, T.; Garcia-Sastre, A.; Caplivski, D.; Cheng, A. C.; Kedzierska, K.; Vapalahti, O.; Hepojoki, J. M.; Simon, V.; Krammer, F. A serological assay to detect SARS-CoV-2 seroconversion in humans. *Nat. Med.* **2020**, *26* (7), 1033−1036.
(33) de Assis, R. R.; Jain, A.; Nakajima, R.; Jasinskas, A.; Felgner, J.; Obiero, J. M.; Norris, P. J.; Stone, M.; Simmons, G.; Bagri, A.; Irsch, J.; Schreiber, M.; Buser, A.; Holbro, A.; Battegay, M.; Hosimer, P.; Noesen, C.; Adenaiye, O.; Tai, S.; Hong, F.; Milton, D. K.; Davies, D. H.; Contestable, P.; Corash, L. M.; Busch, M. P.; Felgner, P. L.; Khan, S. Analysis of SARS-CoV-2 antibodies in COVID-19 convalescent blood using a coronavirus antigen microarray. *Nat. Commun.* **2021**, *12* (1), 6.
(34) Barnidge, D. R.; Dasari, S.; Ramirez-Alvarado, M.; Fontan, A.; Willrich, M. A. V.; Tschumper, R. C.; Jelinek, D. F.; Snyder, M. R.; Dispenzieri, A.; Katzmann, J. A.; Murray, D. L. Phenotyping Polyclonal Kappa and Lambda Light Chain Molecular Mass Distributions in Patient Serum Using Mass Spectrometry. *J. Proteome Res.* **2014**, *13* (11), 5198−5205.
(35) Klein, S. L.; Pekosz, A.; Park, H. S.; Ursin, R. L.; Shapiro, J. R.; Benner, S. E.; Littlefield, K.; Kumar, S.; Naik, H. M.; Betenbaugh, M. J.; Shrestha, R.; Wu, A. A.; Hughes, R. M.; Burgess, I.; Caturegli, P.; Laeyendecker, O.; Quinn, T. C.; Sullivan, D.; Shoham, S.; Redd, A. D.; Bloch, E. M.; Casadevall, A.; Tobian, A. A. Sex, age, and hospitalization drive antibody responses in a COVID-19 convalescent plasma donor population. *J. Clin. Invest.* **2020**, *130* (11), 6141−6150.
(36) Lynch, K. L.; Whitman, J. D.; Lacanienta, N. P.; Beckerdite, E. W.; Kastner, S. A.; Shy, B. R.; Goldgof, G. M.; Levine, A. G.; Bapat, S. P.; Stramer, S. L.; Esensten, J. H.; Hightower, A. W.; Bern, C.; Wu, A. H. B. Magnitude and Kinetics of Anti-Severe Acute Respiratory Syndrome Coronavirus 2 Antibody Responses and Their Relationship to Disease Severity. *Clin. Infect. Dis.* **2021**, *72* (2), 301−308.
(37) Amanat, F.; Stadlbauer, D.; Strohmeier, S.; Nguyen, T. H. O.; Chromikova, V.; McMahon, M.; Jiang, K.; Arunkumar, G. A.; Jurczyszak, D.; Polanco, J.; Bermudez-Gonzalez, M.; Kleiner, G.; Aydillo, T.; Miorin, L.; Fierer, D. S.; Lugo, L. A.; Kojic, E. M.; Stoever, J.; Liu, S. T. H.; Cunningham-Rundles, C.; Felgner, P. L.; Moran, T.; García-Sastre, A.; Caplivski, D.; Cheng, A. C.; Kedzierska, K.; Vapalahti, O.; Hepojoki, J. M.; Simon, V.; Krammer, F. A serological assay to detect SARS-CoV-2 seroconversion in humans. *Nat. Med.* **2020**, *26* (7), 1033−1036.
(38) MacLean, B.; Tomazela, D. M.; Shulman, N.; Chambers, M.; Finney, G. L.; Frewen, B.; Kern, R.; Tabb, D. L.; Liebler, D. C.; MacCoss, M. J. Skyline: an open source document editor for creating and analyzing targeted proteomics experiments. *Bioinformatics* **2010**, *26* (7), 966−8.
(39) Gunn, B. M.; Schneider, J. R.; Shansab, M.; Bastian, A. R.; Fahrbach, K. M.; Smith, A. D.; Mahan, A. E.; Karim, M. M.; Licht, A. F.; Zvonar, I.; Tedesco, J.; Anderson, M. R.; Chapel, A.; Suscovich, T. J.; Malaspina, D. C.; Streeck, H.; Walker, B. D.; Kim, A.; Lauer, G.;

https://doi.org/10.1021/acs.jproteome.1c00882
J. Proteome Res. XXXX, XXX, XXX−XXX

Altfeld, M.; Pillai, S.; Szleifer, I.; Kelleher, N. L.; Kiser, P. F.; Hope, T. J.; Alter, G. Enhanced binding of antibodies generated during chronic HIV infection to mucus component MUC16. *Mucosal Immunol.* **2016**, *9* (6), 1549−1558.

(40) Larsen, M. D.; de Graaf, E. L.; Sonneveld, M. E.; Plomp, H. R.; Nouta, J.; Hoepel, W.; Chen, H.-J.; Linty, F.; Visser, R.; Brinkhaus, M.; Šuštić, T.; de Taeye, S. W.; Bentlage, A. E. H.; Toivonen, S.; Koeleman, C. A. M.; Sainio, S.; Kootstra, N. A.; Brouwer, P. J. M.; Geyer, C. E.; Derksen, N. I. L.; Wolbink, G.; de Winther, M.; Sanders, R. W.; van Gils, M. J.; de Bruin, S.; Vlaar, A. P. J.; Rispens, T.; den Dunnen, J.; Zaaijer, H. L.; Wuhrer, M.; Ellen van der Schoot, C.; Vidarsson, G. Afucosylated IgG characterizes enveloped viral responses and correlates with COVID-19 severity. *Science* **2021**, *371* (6532), No. eabc8378.

(41) Ferrara, C.; Grau, S.; Jäger, C.; Sondermann, P.; Brünker, P.; Waldhauer, I.; Hennig, M.; Ruf, A.; Rufer, A. C.; Stihle, M.; Umaña, P.; Benz, J. Unique carbohydrate-carbohydrate interactions are required for high affinity binding between FcγRIII and antibodies lacking core fucose. *Proc. Natl. Acad. Sci. U. S. A.* **2011**, *108* (31), 12669−74.

(42) Lau, E. H. Y.; Tsang, O. T. Y.; Hui, D. S. C.; Kwan, M. Y. W.; Chan, W. H.; Chiu, S. S.; Ko, R. L. W.; Chan, K. H.; Cheng, S. M. S.; Perera, R.; Cowling, B. J.; Poon, L. L. M.; Peiris, M. Neutralizing antibody titres in SARS-CoV-2 infections. *Nat. Commun.* **2021**, *12* (1), 63.

(43) Anderson, E. J.; Rouphael, N. G.; Widge, A. T.; Jackson, L. A.; Roberts, P. C.; Makhene, M.; Chappell, J. D.; Denison, M. R.; Stevens, L. J.; Pruijssers, A. J.; McDermott, A. B.; Flach, B.; Lin, B. C.; Doria-Rose, N. A.; O'Dell, S.; Schmidt, S. D.; Corbett, K. S.; Swanson, P. A., 2nd; Padilla, M.; Neuzil, K. M.; Bennett, H.; Leav, B.; Makowski, M.; Albert, J.; Cross, K.; Edara, V. V.; Floyd, K.; Suthar, M. S.; Martinez, D. R.; Baric, R.; Buchanan, W.; Luke, C. J.; Phadke, V. K.; Rostad, C. A.; Ledgerwood, J. E.; Graham, B. S.; Beigel, J. H. Safety and Immunogenicity of SARS-CoV-2 mRNA-1273 Vaccine in Older Adults. *N. Engl. J. Med.* **2020**, *383* (25), 2427−2438.

(44) Jackson, L. A.; Anderson, E. J.; Rouphael, N. G.; Roberts, P. C.; Makhene, M.; Coler, R. N.; McCullough, M. P.; Chappell, J. D.; Denison, M. R.; Stevens, L. J.; Pruijssers, A. J.; McDermott, A.; Flach, B.; Doria-Rose, N. A.; Corbett, K. S.; Morabito, K. M.; O'Dell, S.; Schmidt, S. D.; Swanson, P. A., 2nd; Padilla, M.; Mascola, J. R.; Neuzil, K. M.; Bennett, H.; Sun, W.; Peters, E.; Makowski, M.; Albert, J.; Cross, K.; Buchanan, W.; Pikaart-Tautges, R.; Ledgerwood, J. E.; Graham, B. S.; Beigel, J. H. An mRNA Vaccine against SARS-CoV-2 - Preliminary Report. *N. Engl. J. Med.* **2020**, *383* (20), 1920−1931.

(45) Klassen, S.; Senefeld, J.; Senese, K.; Johnson, P.; Wiggins, C.; Baker, S.; van Helmond, N.; Bruno, K.; Pirofski, L.; Shoham, S.; Grossman, B.; Henderson, J.; Wright, S.; Fairweather, D.; Paneth, N.; Carter, R.; Casadevall, A.; Joyner, M. Convalescent Plasma Therapy for COVID-19: A Graphical Mosaic of the Worldwide Evidence. *Front. Med.* **2021**, *8*, 684151.

(46) Galson, J. D.; Schaetzle, S.; Bashford-Rogers, R. J. M.; Raybould, M. I. J.; Kovaltsuk, A.; Kilpatrick, G. J.; Minter, R.; Finch, D. K.; Dias, J.; James, L. K.; Thomas, G.; Lee, W.-Y. J.; Betley, J.; Cavlan, O.; Leech, A.; Deane, C. M.; Seoane, J.; Caldas, C.; Pennington, D. J.; Pfeffer, P.; Osbourn, J. Deep Sequencing of B Cell Receptor Repertoires From COVID-19 Patients Reveals Strong Convergent Immune Signatures. *Front. Immunol.* **2020**, *11*, 605170.

(47) Robbiani, D. F.; Gaebler, C.; Muecksch, F.; Lorenzi, J. C. C.; Wang, Z.; Cho, A.; Agudelo, M.; Barnes, C. O.; Gazumyan, A.; Finkin, S.; Hägglöf, T.; Oliveira, T. Y.; Viant, C.; Hurley, A.; Hoffmann, H.-H.; Millard, K. G.; Kost, R. G.; Cipolla, M.; Gordon, K.; Bianchini, F.; Chen, S. T.; Ramos, V.; Patel, R.; Dizon, J.; Shimeliovich, I.; Mendoza, P.; Hartweger, H.; Nogueira, L.; Pack, M.; Horowitz, J.; Schmidt, F.; Weisblum, Y.; Michailidis, E.; Ashbrook, A. W.; Waltari, E.; Pak, J. E.; Huey-Tubman, K. E.; Koranda, N.; Hoffman, P. R.; West, A. P.; Rice, C. M.; Hatziioannou, T.; Bjorkman, P. J.; Bieniasz, P. D.; Caskey, M.; Nussenzweig, M. C. Convergent antibody responses to SARS-CoV-2 in convalescent individuals. *Nature* **2020**, *584* (7821), 437−442.

(48) Guthals, A.; Gan, Y.; Murray, L.; Chen, Y.; Stinson, J.; Nakamura, G.; Lill, J. R.; Sandoval, W.; Bandeira, N. De Novo MS/MS Sequencing of Native Human Antibodies. *J. Proteome Res.* **2017**, *16* (1), 45−54.

(49) Fornelli, L.; Srzentic, K.; Huguet, R.; Mullen, C.; Sharma, S.; Zabrouskov, V.; Fellers, R. T.; Durbin, K. R.; Compton, P. D.; Kelleher, N. L. Accurate Sequence Analysis of a Monoclonal Antibody by Top-Down and Middle-Down Orbitrap Mass Spectrometry Applying Multiple Ion Activation Techniques. *Anal. Chem.* **2018**, *90* (14), 8421−8429.

(50) Liu, L.; Wang, P.; Nair, M. S.; Yu, J.; Rapp, M.; Wang, Q.; Luo, Y.; Chan, J. F.; Sahi, V.; Figueroa, A.; Guo, X. V.; Cerutti, G.; Bimela, J.; Gorman, J.; Zhou, T.; Chen, Z.; Yuen, K. Y.; Kwong, P. D.; Sodroski, J. G.; Yin, M. T.; Sheng, Z.; Huang, Y.; Shapiro, L.; Ho, D. D. Potent neutralizing antibodies against multiple epitopes on SARS-CoV-2 spike. *Nature* **2020**, *584* (7821), 450−456.

(51) Yamayoshi, S.; Yasuhara, A.; Ito, M.; Akasaka, O.; Nakamura, M.; Nakachi, I.; Koga, M.; Mitamura, K.; Yagi, K.; Maeda, K.; Kato, H.; Nojima, M.; Pattinson, D.; Ogura, T.; Baba, R.; Fujita, K.; Nagai, H.; Yamamoto, S.; Saito, M.; Adachi, E.; Ochi, J.; Hattori, S. I.; Suzuki, T.; Miyazato, Y.; Chiba, S.; Okuda, M.; Murakami, J.; Hamabata, T.; Iwatsuki-Horimoto, K.; Nakajima, H.; Mitsuya, H.; Omagari, N.; Sugaya, N.; Yotsuyanagi, H.; Kawaoka, Y. Antibody titers against SARS-CoV-2 decline, but do not disappear for several months. *EClinicalMedicine* **2021**, *32*, 100734.

(52) Lopez-Santibanez-Jacome, L.; Avendano-Vazquez, S. E.; Flores-Jasso, C. F. The Pipeline Repertoire for Ig-Seq Analysis. *Front. Immunol.* **2019**, *10*, 899.

https://doi.org/10.1021/acs.jproteome.1c00882
J. Proteome Res. XXXX, XXX, XXX−XXX